International Journal of GEOMATE, June, 2026 Vol.30, Issue 142, pp.82-92
ISSN: 2186-2982 (P), 2186-2990 (O), Japan, DOI: https://doi.org/10.21660/2026.142.5422
Geotechnique, Construction Materials and Environment

EVALUATION OF ALUMINOSILICATE REFRACTORY MADE WITH FIRECLAY AND SECONDARY ALUMINIUM DROSS

Doan-Binh Nguyen[1], Doan-Dat Nguyen[1], Van-Hieu Hoang[1] and *Lam Nguyen Trong[1]

[1]Faculty of Building Materials, Hanoi University of Civil Engineering, Hanoi, Vietnam

*Corresponding Author, Received: 07 Jan. 2026, Revised: 26 Feb. 2026, Accepted: 10 March 2026

ABSTRACT: The aluminosilicate refractory material was studied in mixtures of fireclay, chamotte, and secondary aluminium dross. The high content of dross waste was blended, approaching 80% by weight, with fireclay to investigate the influential factors on mould capacity and physico-mechanical properties, which were evaluated based on bulk density, porosity, volume change, water absorption, and cold compressive strength. The aluminium dross, characterized by high porosity and a particle size distribution with a significant proportion under 0.3 mm, significantly influenced moulding parameters, requiring a moisture level of up to 18% and resulting in a reduced bulk density of specimens. The results also indicated that an increase in the amount of aluminium dross raised the porosity and water absorption, but decreased the compressive strength. The performance of the specimens was significantly improved when the maximum size of the aluminium dross particles was reduced from 2.5 mm to 0.3 mm, and the firing temperature was increased from 1400 ˚C to 1450 ˚C. Consequently, the water absorption decreased from 16.6% to 23.5%, and the compressive strength increased by 78.4% to 140%, particularly eliminating the volume-expansive phenomenon in specimens containing the dross waste. Moreover, the microstructure of specimens was also characterized by X-ray diffraction analysis (XRD) and scanning electron microscopy (SEM) techniques.

Keywords: Aluminium dross, Fireclay, Chamotte, Hazardous waste, Refractory

1. INTRODUCTION

Refractories are heat-resistant materials used in almost all processes involving high temperatures and/or corrosive environments [1]. Refractories are nonmetallic materials with chemical and physical properties that make them applicable for structures or as components of systems that are exposed to environments above 538 ˚C [2]. Refractories can be classified by the physicochemical nature of the raw materials used for manufacturing, such as silica, aluminosilicate, and magnesia, or by the nature of the manufacturing process (shaped/unshaped), or by the application temperature, or by their chemical nature (basic, acidic, or neutral) [3, 4]. Aluminosilicate refractories are the most commonly used materials in industrial furnaces, especially in high temperature operating conditions. These materials form a continuous series ranging from siliceous firebricks with 25% Al_2O_3 to corundum bricks with over 90% Al_2O_3 [5]. The temperature withstanding properties of the aluminosilicate refractories largely depend on the alumina content of the system [3].

Aluminium dross is divided into two types, including white dross and black dross. While the white dross is generated by the primary aluminium industry, black aluminium dross, also known as secondary aluminium dross, is skimmed from the top float layer of the melting liquid of aluminium scraps, such as beverage cans, commercial scraps, and castings, and contains a large amount of salt flux [6]. Generally, the secondary aluminium dross was received approximately 150 – 300 kg per ton of recovered aluminium, depending on the scrap feeding. The black dross commonly compounds with low alumina content, high amounts of metal oxides, aluminium nitride, and salt flux [1, 6]. The secondary aluminium dross is a hazardous waste because it comes in contact with water, producing toxic and flammable gases such as NH_3, H_2, CH_4, PH_3, and H_2S [7]. Several chemical reactions of aluminium compounds were contacted with water or moist air [8]. According to the investigated information, the dross content can be generated by approximately 0.2–0.3% of waste aluminium products during the recycling process. Most of the waste is directly disposed of in landfills without treatment. The heavy metals and salts leach into water and soil, causing environmental pollution [9]. The heavy oxide contamination is often based on Pb, Cr, Cu, and Zn, which directly influence the organic matter and soil pH. The pollution links clearly to the serious medical conditions such as cancer, liver damage, skin rashes, and reproductive disorders [1]. In Vietnam, the impacts of the aluminium recycling process on the living environment have been recorded for many years, particularly in the craft villages. Consequently, the accumulation of huge amounts of dross waste has significantly influenced living conditions and the health of many people, leading to various diseases related to pollution.

It is necessary to mitigate the environmental impact of aluminium dross waste. Hence, an environmental management system of the aluminium production industry was studied by Sajwani et al. [10].

Among the solution ways, utilizing the aluminium dross will have numerous benefits, such as conserving many natural material sources, reducing the energy consumption of the sintering process, and lowering the manufacturing process cost. Yoshimura et al. [11] utilized white aluminium dross from plasma reactor processing to produce the refractories. The specimens were fired up to 1450 ˚C, and their physico-mechanical properties, including flexural strength, compressive strength, shrinkage, bulk density, and apparent porosity, were analyzed. In another study, Li et al. [12] mixed the dross waste of blast furnace with two particle sizes (1–3 mm and <1 mm) and phenolic resin as an adhesive to produce high-alumina refractories. The specimens sintered to a maximum temperature of 1550 ˚C for three hours were also tested on the physico-mechanical properties. The waste from aluminium rolling mills was blended with clay, kaolin, or bentonite to produce refractory bricks by Adeosun et al. [1, 6]. Additionally, Shi et al. reported that primary aluminium dross can be used to fabricate periclase and magnesium aluminate spinel refractories by adding magnesium oxide [13]. According to the literature review, most studies only have been focused on utilizing the white dross, while lack of the hazardous waste of aluminium recycling was investigated in making eco-friendly refractory bricks, especially considering the volume change of specimens.

In this study, secondary aluminium dross was blended with fireclay and chamotte to produce an aluminosilicate refractory brick. Influencing factors, such as dross waste content, moisture, pressure, particle size, and sintering temperature, on mould capacity and physico-mechanical properties were investigated for evaluating the recyclable capacity of untreated dross waste as inexpensive method. The study provided the optimum conditions of influential factors on the moulding capacity, including moisture and pressure. Moreover, the mechanical properties were investigated with different contents of aluminium dross, approaching 80% by mass, in various mix proportions. The outcomes were considered as potential ways to produce eco-friendly materials from the hazardous waste of secondary aluminium recycling, contributing to sustainable development by conserving natural resources and protecting the environment from pollution.

2. RESEARCH SIGNIFICANCE

The study provided the potential ways to improve the performance of refractory bricks containing the secondary aluminium dross. The conventional solution was investigated on the mix proportions combining the fireclay, dross waste, with chamotte particles as a major role in restricting the volume expansion. Moreover, the properties of aluminosilicate specimens was significantly improved with a decrease in particle size of the dross and an increase in sintering temperature. Consequently, an increase in the volume shrinkage corresponds to the mechanical properties of mix proportions, particularly high content of aluminium dross up to 80% by mass.

3. EXPERIMENT STUDY

3.1 Materials and Mix Proportions

Fig. 1 shows the primary materials used in the experimental program, including the secondary aluminium dross, fireclay, and chamotte. The physical properties and chemical composition of these materials are summarized in Tables 1 and 2, respectively. According to the chemical composition, the dross contains high alumina, exceeding 66%, which is a good source for making refractory bricks. The dross wasted from an aluminium recycling craft village had a dark grey colour and an ammoniac odour. The material was dried and screened to remove particle sizes larger than 2.5 mm, which had distribution curves as presented in Fig. 2. According to this analysis, the aluminium dross only had large particle size over 0.3 mm up to 95%, which would significantly affect the density of specimens. Moreover, the bulk density and specific density of the dross waste were tested at only 0.9 g/cm^3 and 1.88 g/cm^3, while the water absorption was relatively high, reaching up to 33.8%. These results indicated that the dross waste was composed of light particles and contained numerous open pores in the structure. The morphology of the dross waste with various crystals and the microstructure of the particle surface were also observed clearly by SEM analysis, (Fig. 3), as following:

- The small particles were agglomerated together to form larger ones with random shapes;
- High porosity with various sizes existed among the particles.

As shown in the results of the XRD analysis in Fig. 4, the components of aluminium dross are complex, comprising different phases. In which γ-alumina and corundum phases had the primary concentration with 68.6% and 24.2%, respectively. The last phases of the dross waste included chabazite-Ca, aluminium, quartz, boggsite, and hydrated alumina, as listed in Table 3.

Table 1. Physical properties of materials

Materials	Bulk density (g/cm^3)	Specific density (g/cm^3)	True porosity (%)	Water absorption (%)
Aluminium dross	0.90	1.88	52.1	33.8
Fireclay	1.17	2.54	53.9	-
Chamotte	1.38	2.62	47.3	15.5

Fireclay powder and chamotte were used as the local refractory company supplied standard material. The fireclay had a bulk density of 1.17 g/cm^3, a specific density of 2.54 g/cm^3, and a plasticity index of 7.2. Besides, the chamotte had a bulk density of 1.38 g/cm^3, a specific density of 2.62 g/cm^3, and a nominal maximum size of 2.5 mm. The water absorption of chamotte was 54.1% lower than that of the dross waste. Besides, the chamotte possessed a high content of particle size under 0.3 mm, approaching nearly 40% by mass, as presented in Fig. 2.

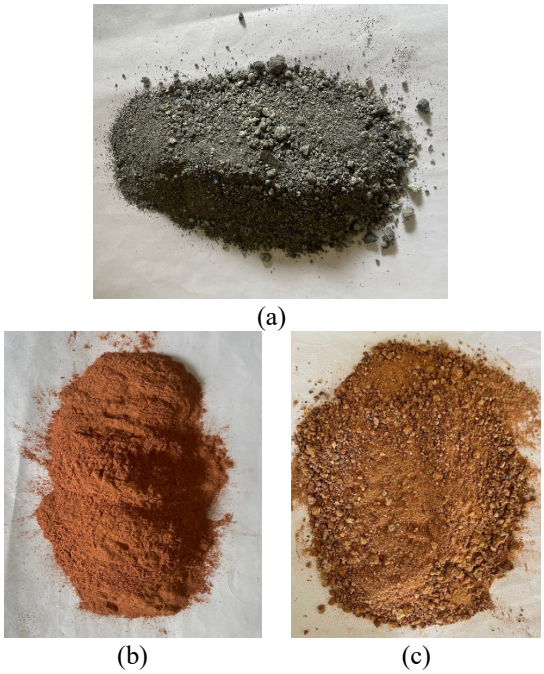

(a) (b) (c)

Fig. 1 Raw materials: (a) secondary aluminium dross; (b) fireclay; and (c) chamotte

As shown in Table 4, total 10 mixes were designated to investigate the aluminium dross on the physico-mechanical properties of specimens. The mix proportions were calculated on the alumina contents, which should cover the requirements for fireclay and high-alumina refractories as ASTM C27-98(2022) [14]. The control mix CH70-2.5 combined only 30% fireclay and 70% chamotte, with a maximum particle size of 2.5 mm. In contrast, mixes A15C55, A30C40, and A45C25 partially replaced the chamotte content with aluminium dross, at ratios of 15%, 30%, and 45% by weight, respectively. These mix proportions had the alumina contents from about 25% to 47% and were sintered in an electric furnace at 1400 ˚C for three hours.

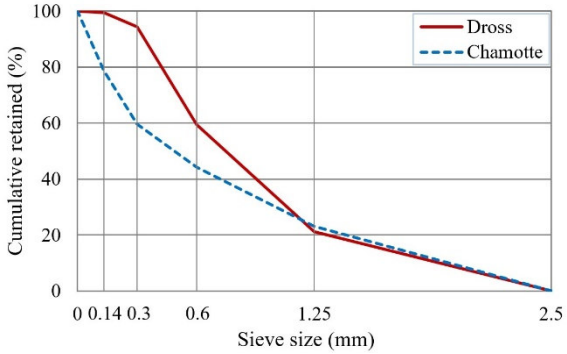

Fig. 2 Particle-size distribution of materials

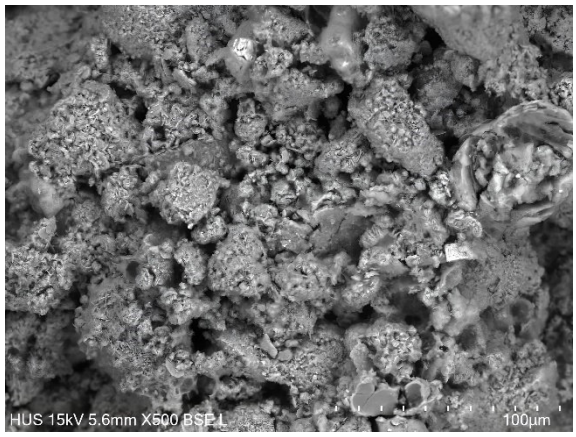

Fig. 3 SEM of secondary aluminium dross

The last six mixes used a varied content of aluminium dross, ranging from 60% to 80% by weight, corresponding to a reduction in fireclay content from 40% to 20% by weight. In the mix proportions using dross waste and fireclay, the alumina content, after removing the loss on ignition (LOI), attained high values in the 53.8% and 63.6% range. These values satisfied the criteria of high-alumina refractory brick with the alumina content at least 50% by mass as guidelines of ASTM C27-98(2022) [14]. Moreover, the combination of dross waste and fireclay also gives more benefits, such as an increase in consumption of hazardous material and simplification of the manufacturing process. To investigate the influence of particle sizes and sintering

Table 2. Chemical composition of materials

Materials	Chemical composition (% by mass)								
	SiO_2	Al_2O_3	TiO_2	Fe_2O_3	CaO	MgO	Na_2O	K_2O	LOI
Aluminium dross	3.70	66.76	0.00	2.28	1.31	3.69	13.09	0.00	9.16
Fireclay	58.55	23.26	2.38	8.10	0.00	1.16	0.00	2.44	4.11
Chamotte	62.08	25.54	1.52	5.49	3.00	0.00	0.00	2.37	0.00

temperatures on the properties of specimens, two maximum sizes (D_{max}) of the aluminium dross particles were used, namely 2.5 mm and 0.3 mm, corresponding to firing temperatures of 1400 ˚C and 1450 ˚C. The adjustment of both a decrease in the particle size and an increase in the temperature has the main purpose to improve the sintering process of specimens.

3.2 Experimental procedures

The experimental procedure was summarized as shown in Fig. 5. All raw materials were carefully prepared to represent of the selected lot, particularly the dross waste, which has high heterogeneous components. The representative samples ensured the complete range of colours, particles, and textures before the testing process per the guidelines of ASTM

Table 3. X-ray diffraction analysis of aluminium dross

Crystalline phase	Chemical formula	Concentration (%)	Crystal information		
			Crystal system	Space group	Molar ratio (%)
γ-alumina	Al2.67 O4	68.6	Cubic	227 : Fd-3m	84.6
Corundum	Al2 O3	24.2	Trigonal(H)	167 : R-3c	6.6
Chabazite-Ca	Al0.76 H10 O12.247 Si3.24	0.56	Orthorhombic	74 : Imma	0.0163
Aluminium	Al	2.0	Cubic	225 : Fm-3m	3.2
Quartz	O2 Si1	1.72	Trigonal(H)	152 : P3121	4.8
Boggsite	Al0.32 O2 Si0.68	1.4	Trigonal(R)	166 : R-3m	0.33
Hydrated alumina	5[Al2O3]*H2O	1.39	Hexagonal	186 : P63mc	0.44

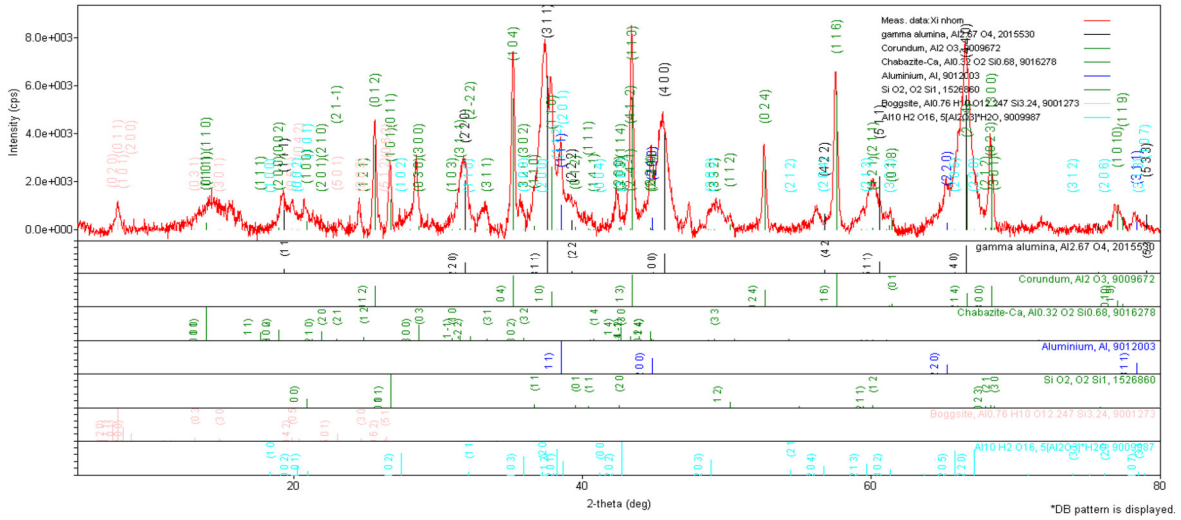

Fig. 4 X-ray diffraction of aluminium dross

Table 4. Mix proportions

Mix	Materials (% by mass)			Maximum particle size (mm)	Al_2O_3 (%)	Optimum moulding		Sintered temperature (˚C)
	Fireclay	Aluminium dross	Chamotte			Moisture (%)	Pressure (MPa)	
C70-2.5	30	0	70	2.5	25.2	8	4.0	1400
A15C55	30	15	55	2.5	32.3	12	6.0	1400
A30C40	30	30	40	2.5	39.5	12	9.2	1400
A45C25	30	45	25	2.5	46.7	12	15.2	1400
A60-2.5	40	60	0	2.5	53.8	18	13.8	1400
A70-2.5	30	70	0	2.5	58.7	18	16.0	1400
A80-2.5	20	80	0	2.5	63.6	18	24.0	1400
A60-0.3	40	60	0	0.3	53.8	18	14.8	1450
A70-0.3	30	70	0	0.3	58.7	18	18.2	1450
A80-0.3	20	80	0	0.3	63.6	18	24.0	1450

C67/C67M-21 [15]. The aluminium dross was sieved to remove particles larger than 2.5 mm, while the other was crushed in a ball mill and then screened to limit the maximum size to 0.3 mm. The chamotte was also screened to discard particles larger than 2.5 mm. These materials were blended with fireclay based on designated mix proportions. The mixes were added water, which was calculated on the absolute moisture values by mass of the tested specimens. The water content was sprayed uniformly on the dry materials of mix proportion. Next step, these mixes were sealed in a plastic bag for 24 h before moulding 50 × 50 × 50-mm cubic specimens by a hydraulic machine. After drying at 105 ˚C ± 5 ˚C until the constant weight, the real moisture, bulk density and volume change were determined. The specimens were sintered in an electric furnace with a heating rate of approximately 5 ˚C/min, which reached the maximum temperature in the range of 1400–1450 ˚C within 4.5 h and was maintained at the final temperature for the next three hours. The cooling process of specimens occurred naturally to room temperature after the furnace shutdown. The mixes with three ingredients, including fireclay, aluminium dross, and chamotte, were sintered at 1400 ˚C, as illustrated in Fig. 6. The results demonstrated the improvement of mixes incorporating the aluminium dross. An increase in the dross content up to 45% corresponding to the alumina in the range of 25.2% to 46.7%. Consequently, the specimens colour was being converted from grey to yellow.

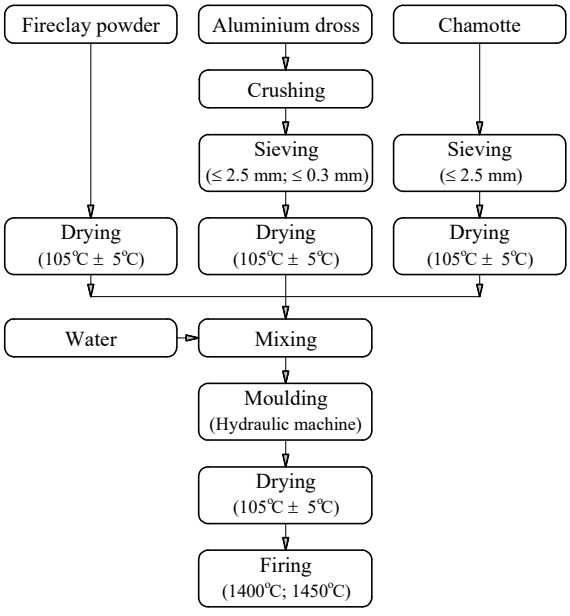

Fig. 5 Process diagram of experimental study

The mechanical properties were determined on at least of three specimens for each testing per guidelines of standard. The cold compressive strength was measured on 50 × 50 × 50-mm cubic specimens according to ASTM C133-97(2021) [16], while the bulk density, porosity, and water absorption were evaluated as specified in TCVN 6530-3:2016 [17]. Additionally, the specific density of the specimens was determined using the Le Chatelier Flask apparatus according to the guidelines of TCVN 6530-2:2016 [18], and the permanent volume change was measured in accordance with TCVN 6530-5:2016 [19]. The microstructure of specimens was also characterized by X-ray diffraction analysis (XRD) and scanning electron microscopy (SEM) techniques.

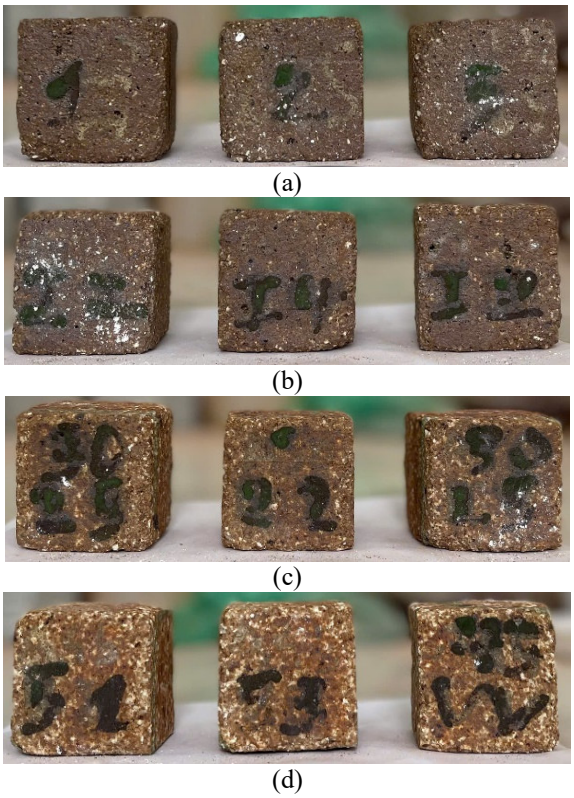

Fig. 6 Sintered specimens: (a) C70-2.5; (b) A15C55; (c) A30C40; and (d) A45C25

4. RESULTS AND DISCUSSION

4.1 Effect of factors on moulding pressure

4.1.1 Aluminium dross

As shown in Table 4, the moulding press of control mix C70-2.5, which has a bulk density of 2.00 g/cm^3 and a moisture content of 8%, was only 4 MPa. However, when the aluminium dross was added partially to replace the chamotte content with ratios in the range of 15% to 45% by mass, the pressure was increased from 6 MPa to 15.2 MPa, based on a water content of 12%, respectively. The reason could be explained by the high water absorption of the aluminium dross compared to that of chamotte. Therefore, the connective capacity of particles was reduced as the higher the dross waste, the smaller the chamotte. Consequently, an increase in pressure was

required to cohere the particles in the moulding process.

The moulding pressure of specimens using aluminium dross with a maximum particle size of 0.3 mm is shown in Fig. 7. In this investigation, all specimens had a fixed bulk density of 2.00 g/cm^3. The pressure was observed to rise approximately from 29% to 62%, depending on the different moulding moistures, and an increase in the dross content of 60–80%. It is clearly seen that an increase in the content of dross waste, which had a high water absorption of 33.8%, also required more water content for mouldability.

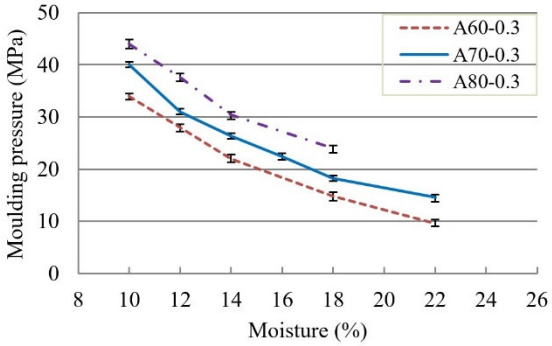

Fig. 7 Effect of aluminium dross on moulding pressure

4.1.2 Moisture

The A70-2.5 mix consisted of 70% aluminium dross combined with 30% fireclay, which was the mean value among the designated mixes. Therefore, this mix was chosen to investigate the influential factors on moulding pressure, such as moisture and bulk density. As shown in Fig. 8, the moulding pressure had a negative correlation with the increase in water content added to the mixes. The pressure values were reduced significantly, approximately 67%, when the water was changed from 12% to 18%. Then, the pressure was slightly affected by water, increasing by 18% to 24%. The influence of water on pressure could be explained by reducing internal friction, which plays a significant role in enhancing the dispersion of particles and impacting the mouldability of the particles themselves. Moreover, the water also improved the plasticity of the fireclay, allowing the aluminium dross particles to be closely connected together under compaction pressure. However, if the water is added excessively, the clay will be converted to a suspension state, which reduces the plasticity property. This issue could reduce the influence of water role in mouldability under semi-dry pressure. The bulk density of specimens also impacted the relationship between moisture and moulding pressure. When the bulk density was changed from 1.80 g/cm^3 to 2.10 g/cm^3, the moulding pressure increased by 224% to 540%, corresponding to water contents of 18% and 24%, respectively. It is clearly seen that an increase in density reduced the slip capacity of the particles in the mould.

According to the experimental results on the specimen using aluminium dross and fireclay, the optimum moulding values were selected for further analysis, including a bulk density of 2.00 g/cm^3 and a moisture content of 18%. This decision was also considered carefully on the influence of moulding conditions on the energy consumption and equipment wear of the hydraulic machine. It can be seen clearly that an increase in moulding pressure requires more power due to higher frictional resistance and longer cycle time in making the specimens, particularly holding times of maximum stress. Moreover, the higher pressure increases the interaction between the raw materials and mould surfaces, which will damage the equipment wear. The optimum moulding pressure of specimens was summarized in Table 4. As the results, the moulding pressure of the specimens using the maximum particles of 2.5 mm with 70% and 80% aluminium dross was increased by 16–74% higher than that of the mix containing 60% aluminium dross. Additionally, the mixes with the maximum particle size of 0.3 mm, including A70-0.3 and A80-0.3, increased the pressure from 23% to 62% compared to the mix A60-0.3. These values show that particle size has a slight influence on the moulding capacity.

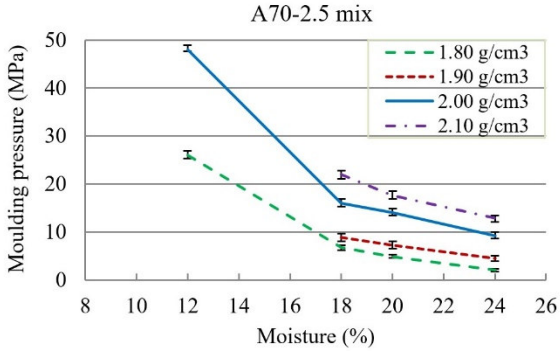

Fig. 8 Effect of moisture and bulk density on moulding pressure

4.2 Effect of aluminium dross content on physico-mechanical properties

The physico-mechanical properties of specimens were analysed based on bulk density, true porosity, apparent porosity, volume change, water absorption, and compressive strength at room temperature, as summarized in Table 5.

4.2.1 Density and porosity

The bulk density of unfired specimens with a moisture content of 0% was alternated in the range of 1.59 g/cm^3 to 1.87 g/cm^3, while that of sintered mixes was between 1.45 g/cm^3 and 1.75 g/cm^3. These values are less significant than the required bulk density of fireclay and high-alumina refractory brick, at least

2.20 g/cm^3 [14], but the specimens using a high content of dross waste of at least 60% might satisfy the criteria of the insulating firebrick with the maximum bulk density of 1.52 g/cm^3, as guidelines of ASTM C155-97(2022) [20]. According to the experimental research shown in Fig. 9, the bulk density of the sintered specimens, including A15C55, A30C40, and A45C25, decreased slightly by 4%, 5.7%, and 8%, respectively, compared to the control mix C70-2.5. These values resulted from replacing lower-density aggregates in the mix composition.

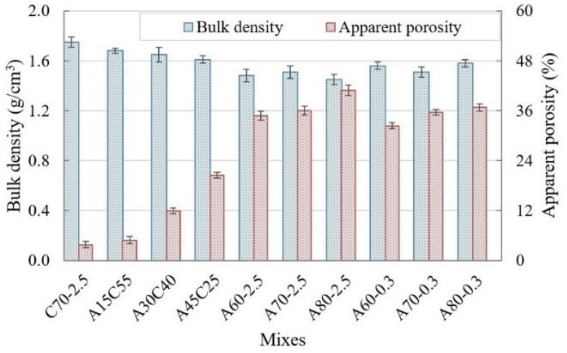

Fig. 9 Effect of aluminium dross on bulk density and apparent porosity

The specific density of all sintered specimens was determined to be nearly 2.79 g/cm^3, consequently, the true porosity was calculated with the values as presented in Table 5. The mixes exhibited a true porosity increase in the range of 6.7% to 13.5%, while the apparent porosity increased nearly 440% compared to the control mix C70-2.5. The results indicated that an increase in the aluminium dross content also raised the porosity of specimens, especially the apparent porosity of mixes combining fireclay, dross waste, and chamotte. The key reason could be attributed to the highly porous dross particles, which comprise a large proportion of the mix composition. On the other hand, the mixes containing the aluminium dross in the range of 60 – 80% by mass had a small gap between the true porosity and apparent porosity, with maximum values of 21.8% and 11.7% corresponding to the mixes containing the maximum particles of 2.5 mm and 0.3 mm, respectively. Therefore, the sealed pores of specimens containing the aluminium dross were significantly lower than those of the mixes using chamotte.

4.2.2 Volume change

The volumes of mixes A15C55, A30C40, and A45C25 were reduced by 0.6%, 0.99%, and 1.18%, respectively, while that of the control decreased by 0.4%, as shown in Table 5. The results indicated that the sintering process occurred well at a temperature of 1400 ˚C with mixes containing chamotte and aluminium dross. One of the key reasons could be the early formation of the liquid phase due to the presence of numerous impure substances, which speeds up the chemical reactions at high temperatures [21]. Then, the pores were filled with the liquid phase, resulting in an increase in sintered density as a consequence of the shrinkage phenomenon that occurred, particularly in specimens with a high content of aluminium dross.

When the maximum particle size of the aluminium dross was reduced from 2.5 mm to 0.3 mm, and the sintering temperature increased from 1400 ˚C to 1450 ˚C, the quality of the specimens was significantly improved based on the compared values, such as volume change, water absorption, and compressive strength. The volumes of specimens A(60–80)-2.5 were expanded by 0.85% to 1.08%. The expansive phenomenon of specimens was likely due to additional mullite formation ($3Al_2O_3.2SiO_2$) and parallel growth of corundum crystals within the aluminium dross aggregates through a recrystallization process [4]. In contrast, the volumes of specimens A(60–80)-0.3 exhibited shrinkage, ranging from 0.98% to 1.06%. The shrinkage resulted in a uniform structure of crushed aluminium dross with low residual porosity. Furthermore, the sintering process of smaller dross particles occurred more easily than that of larger ones. An increase in the final

Table 5. Properties of specimens

Mix	Bulk density of unfired specimen (g/cm^3)	Sintered specimens					
		Bulk density (g/cm^3)	True porosity (%)	Apparent porosity (%)	Volume change (%)	Water absorption (%)	Compressive strength (MPa)
C70-2.5	1.87	1.75	37.3	3.8	-0.40	2.1	29.2
A15C55	1.75	1.68	39.8	4.9	-0.60	2.8	27.8
A30C40	1.74	1.65	40.9	11.9	-0.99	6.6	24.8
A45C25	1.72	1.61	42.3	20.5	-1.18	11.9	18.8
A60-2.5	1.61	1.48	47.0	34.8	+0.86	27.2	12.5
A70-2.5	1.65	1.51	45.9	36.0	+1.08	28.3	11.2
A80-2.5	1.59	1.45	48.0	41.0	+0.83	31.2	8.0
A60-0.3	1.64	1.56	44.1	32.4	-1.05	20.8	22.3
A70-0.3	1.63	1.51	45.9	35.6	-0.98	23.6	20.8
A80-0.3	1.66	1.58	43.4	36.8	-1.06	24.4	19.2

temperature up to 1450 °C also improved the growth of mullite crystals [21, 22].

4.2.3 Water absorption

As shown in Fig. 10, the water absorption increased with an increase in the aluminium dross content. Notably, a clear increase in water absorption was observed in mixes using dross waste at a range of 15% to 45% compared with the control mix C70-2.5. The water absorption of mixes A15C55, A30C40, and A45C25 was 2.8%, 6.6%, and 11.9%, respectively, corresponding to apparent porosity values of 4.9%, 11.9%, and 20.5%. On the other hand, the water absorption and apparent porosity of control mix C70-2.5, which contained no dross waste, were only 2.1% and 3.8%, respectively. The testing data demonstrated the influence of highly open porosity of the aluminium dross on sintered specimens.

When the aluminium dross increased from 60% to 70% and 80%, the water absorption of A70-2.5 and A80-2.5 was approximately 4% and 15% higher than that of A60-2.5. Additionally, the water absorption values of mixes A70-0.3 and A80-0.3 increased from 13.5% to 17.3%, compared to mix A60-0.3. The water absorption values are directly related to the porosity of the specimens, which increased depending on the amount of aluminium dross, as presented in Table 5. When the temperature was raised to 1450 ˚C, the specimens containing the maximum particles of 0.3 mm had lower water absorption than those fired at 1400 ˚C with the maximum particles of 2.5 mm. The results indicated that the water absorption of the specimens A(60–80)-0.3 was notably lower, ranging from 16.6% to 23.5%, compared to the last ones, including A(60–80)-2.5.

4.2.4 Compressive strength

The inverse proportion between compressive strength and water absorption is clearly shown in Fig. 10. When the compressive strength of specimens using aluminium dross under 45% by mass was decreased from 29.2 MPa to 18.8 MPa, the water absorption increased in the range of 2.1% to 11.9% corresponding the raise of the apparent porosity between 3.8% and 20.5%. Similar trends were also observed in specimens containing 60–80% aluminium dross. In these mixes, the strength of specimens was reduced by at least 14%, while the apparent porosity was varied slightly from 14% to 18%. Sittiakkaranon et al. [23] reported that the alumina content impact directly on the physical characterization of refractories. The results demonstrate the direct influence of water absorption, which is closely related to apparent porosity, on the compressive strength of specimens. However, these properties of specimens did not meet the criteria of dense aluminosilicate refractory bricks, which required the cold compressive strength at least 30 MPa and the apparent porosity under 24% [24, 25]. This issue also means that an increase in the dross content requires a higher firing temperature for good sintering of specimens.

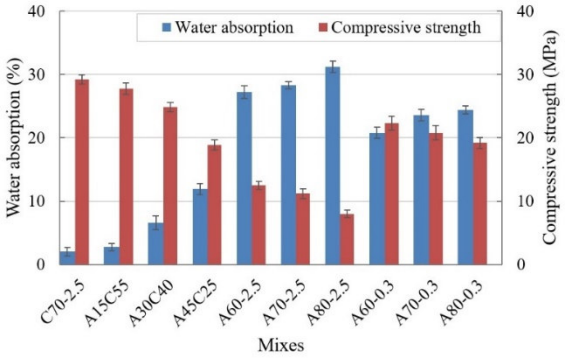

Fig. 10 Effect of aluminium dross on water absorption and compressive strength

The compressive strength was significantly improved due to a decrease in maximum particle sizes and an increase in sintering temperature. The strength of specimens A(60–80)-0.3 was higher, ranging from 78.4% to 140%, compared to the last specimens containing the maximum particles size of 2.5 mm, which had the same contents of aluminium dross, from 60% to 80%. The compressive strength was increased due to the larger amount of fine particles filling the voids of the specimens, as found by Li et al [12]. The increase in mullite crystals formed during the higher temperature process could be the reason for the development of compressive strength. This observation also agrees with the study by Lukita et al. [7]. Besides, Yeh et al. [26] found that an increase in temperature will raise the amount of alumina, especially in the α-Al_2O_3 phase. Conversely, the decrease in strength of specimens A(60–80)-2.5, which resulted in an expansion of volume, could be associated with increased water absorption and porosity. This relationship between cold compressive strength and porosity ratio was similar to that observed in research conducted by Amkpa et al. [27].

4.3 Microstructure analysis

4.3.1 X-ray diffraction

Fig. 11 shows the XRD pattern of the A70-2.5 mix sintered at 1400 ˚C, which includes green, black, and blue lines, denoting corundum, mullite, and SiO_2 (as a glass or vitrified phase), respectively. These phases are intrinsic to the aluminosilicate refractory. The different phases could be confirmed by the appearance of the peaks with Miller indices (h, k, l), which indicate the orientation of a plane or set of parallel planes of atoms in a crystal. A minor concentration belonged to SiO_2 with only 8.8%, as presented in Table 6, while the main crystalline phases were

Table 6. X-ray diffraction analysis of A70-2.5 mix

Crystalline phase	Chemical formula	Concentration (%)	Crystal information		
			Crystal system	Space group	Molar ratio (%)
Corundum	Al2 O3	46.9	Trigonal(H)	167 : R-3c, hexagonal	61.7
Mullite	Al2.25 O4.871 Si0.75	44.3	Orthorhombic	55 : Pbam	18.6
Quartz	O2 Si1	8.8	Triclinic	1 : P1	19.7

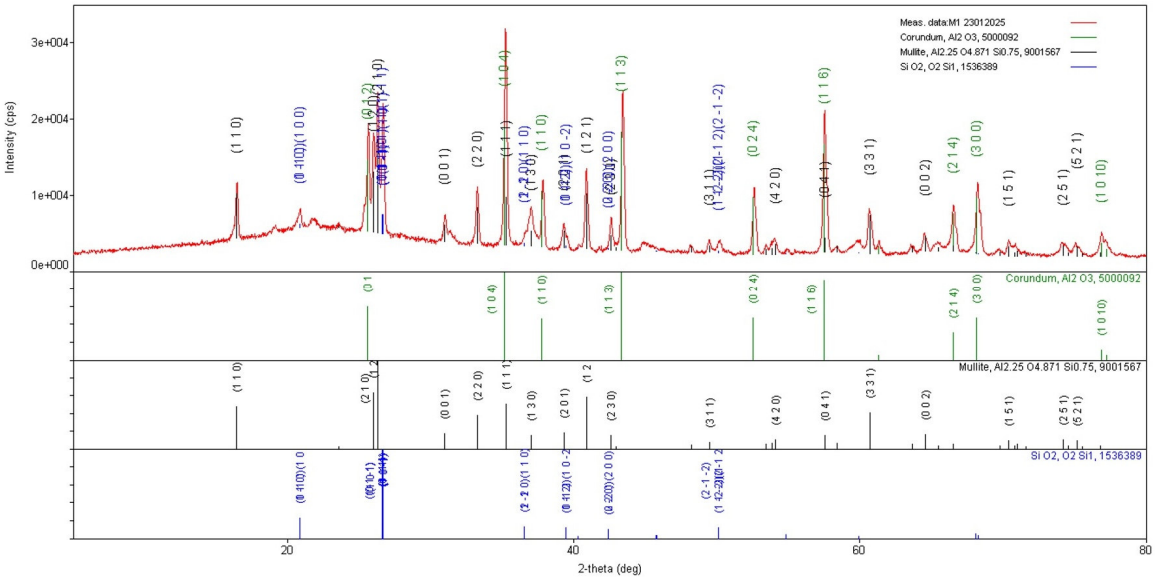

Fig. 11 X-ray diffraction of A70-2.5 mix

mullite $3Al_2O_3.2SiO_2$ and corundum Al_2O_3, corresponding to 44.3% and 46.9%. The transformation of the quartz phase was only observed until temperatures of about 1250 ˚C. The amount of high-silica quartz solution was increased at higher temperatures. Even quartz particles smaller than 20 µm could completely dissolve at approximately 1350 ˚C [28]. Fine mullite needles appear at approximately 1000 ˚C but cannot be resolved with an optical microscope until sintering temperatures of at least 1250 ˚C are reached. At high temperatures (1200 – 1300˚C), Al_2O_3 reacts with SiO_2 as follows [22].

$$3\left(Al_2O_3.2SiO_2\right) \rightarrow 3Al_2O_3.2SiO_2 + 4SiO_2 \quad (1)$$

$$3Al_2O_3 + 2SiO_2 \rightarrow 3Al_2O_3.2SiO_2 \quad (2)$$

After firing above 1400 ˚C, mullite is present as prismatic crystals up to about 0.01 mm in length, as shown in Fig. 12. The mullite crystal is composed of 71.8% Al_2O_3 and 28.2% SiO_2 by weight. The amount of developed mullite phase depends on the total alumina content of the mix proportion. This phase exhibited outstanding properties of the refractory, including high thermal and chemical stability, excellent creep resistance, and fracture toughness, which were directly affected by the percentage of mullite present [29]. Additionally, corundum is a crystalline form of aluminium oxide (Al_2O_3) formed when molten aluminium reacts with aluminosilicate. The corundum crystal exhibits excellent chemical stability, high heat resistance, and exceptional hardness. The identified phases contribute to the thermal and mechanical performance of aluminosilicate refractory materials due to their prominent features, such as high density, melting point, fracture toughness, and strength, as presented in the report by Cui et al. [30].

4.3.2 Scanning electron microscopy

The microstructure of the A70-2.5 mix was further analyzed by SEM, which was taken at 6000x magnification, as shown in Fig. 12. The main features of A70-2.5 mix observed from the SEM analysis could be listed as:

- The needle-shaped crystals of mullite has sizes up to 8–10 µm;
- The micropores, with various shapes and sizes, were distributed randomly throughout the specimens. Some macropores had large size up to 0.1 mm.

The larger mullite needles grow into the liquid phase. The development of mullite crystals was also controlled by further increases in temperature. In another study, Aksel [31] indicated that the needle-like mullite particles improve pull-out and crack deflection, particularly the high resistance to thermal shock. Besides, the trigonal crystals of corundum were

scattered in the microscopy image. The amount of corundum phase depends on the sintering temperature, the duration of thermal treatment, and the chemical composition, including alkali oxides and iron oxides, which create melting points at low temperatures. This is a necessary condition for forming corundum crystals. In general, the conversion of corundum structure occurs when heating above 1300 ˚C, and the γ-Al_2O_3 form is changed to α-Al_2O_3 [32].

The existence of pores was primarily caused by the evolution of gas during physicochemical reactions during thermal processing. The pores were an indispensable part of the total components, which influence the physico-mechanical properties of specimens, such as the bulk density, water absorption, and strength.

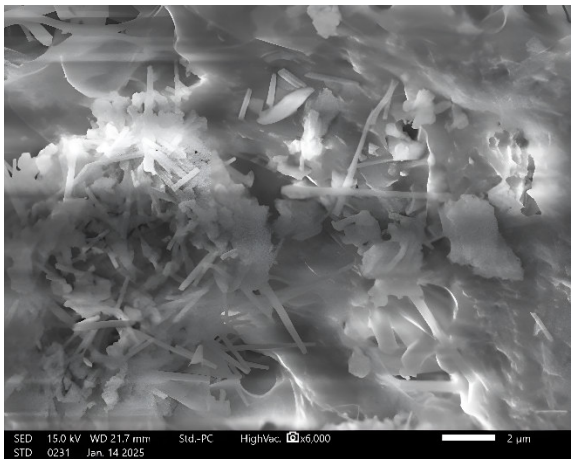

Fig. 12 SEM of A70-2.5 mix

5. CONCLUSIONS

The experiment was conducted on aluminosilicate refractories using secondary aluminium dross. According to the investigated results, the following conclusions can be drawn:

- The aluminium dross possessed high porosity and a lack of particle size under 0.3 mm, which significantly affected the moulding parameters with required moisture up to 18%. Besides, the lowest bulk density of the dried and sintered specimens attained 1.59 g/cm^3 and 1.45 g/cm^3, respectively.
- An increase in the dross waste content required a higher firing temperature, which was evaluated on sintered specimens, including colour, apparent porosity, water absorption, and cold compressive strength.
- The performance of the mixes was significantly improved based on a decrease in the maximum size of aluminium dross particles from 2.5 mm to 0.3 mm and an increase in the sintered temperature up to 1450 ˚C. As a result, the shrinkage volume of the specimens was improved, corresponding to a decrease in water absorption from 16.6% to 23.5% and an increase in compressive strength of 78.4% to 140%.

6. ACKNOWLEDGMENT

The first author acknowledges the financial support of Hanoi University of Civil Engineering under grant number 19-2024/KHXD-TD.

7. REFERENCE

[1] Adeosun S., Akpan E., and Dada M., Refractory characteristics of aluminum dross-kaolin composite, The Minerals, Metals & Materials Society, 66(11), 2014, pp.2253-2261. https://doi.org/10.1007/S11837-014-1179-5

[2] ASTM C71-12(2018), Standard terminology relating to refractories, ASTM, West Conshohocken, 2018.

[3] Dana K., Sinhamahapatra S., Tripathi H. S., and Ghosh A., Refractories of Alumina-Silica System, Transactions of the Indian Ceramic Society, 73(1), 2014, pp.1-13. https://doi.org/10.1080/0371750X.2014.905265

[4] Schacht C.A., Refractories handbook, New York: Marcel Dekker, 2004.

[5] Chesters J., Refractories: Production and Properties, London: The Iron and Steel Institute, 1973.

[6] Adeosun S.O., Sekunowo O.I., Taiwo O.O., Ayoola W. A., and Machado A., Physical and mechanical properties of aluminum dross, Advances in Materials, 3(2), 2014, pp.6-10. https://doi.org/10.11648/j.am.20140302.11

[7] Lukita M., Abidin Z., Riani E., and Ismail A., Utilization of hazardous waste of black dross aluminum: processing and application-a review, Journal of degraded and mining lands management, 9(2), 2022. https://doi.org/10.15243/jdmlm.2022.092.3265

[8] Tsakiridis P., Aluminium salt slag characterization and utilization – A review, Journal of Hazardous Materials, Vols. 217-218, 2012, pp.1-10. https://doi.org/10.1016/j.jhazmat.2012.03.052

[9] Lou B., Shen H., Liu B., Liu J., and Zhang S., Recycling secondary aluminum dross to make building materials: A review, Construction and Building Materials, vol. 409, 2023.https://doi.org/10.1016/j.conbuildmat.2023.133989

[10] Sajwani A., and Nielsen Y., The application of the environmental management system at the aluminum industry in UAE, International Journal of GEOMATE, 12(30), 2017, pp.1-10. https://doi.org/10.21660/2017.30.80102

[11] Yoshimura H., Abreu A., Molisani A., Camargo A.D., Portela J., and Narita N.,

Evaluation of aluminum dross waste as raw material for refractories, Ceramics International, vol. 34, 2008, pp. 581-591, 2008. https://doi.org/10.1016/j.ceramint.2006.12.007

[12] Li A., Zhang H., and Yang H., Evaluation of aluminum dross as raw material for high-alumina refractory, Ceramics International, vol. 40, 2014, pp.12585-12590. https://doi.org/10.1016/j.ceramint.2014.04.069

[13] Shi M., Li Y., and Shi J., Fabrication of periclase and magnesium aluminate spinel refractory from washed residue of secondary aluminum dross, Ceramics International, vol. 48, 2022, pp.7668-7676. https://doi.org/10.1016/j.ceramint.2021.11.312

[14] ASTM C27-98(2022), Standard classification of fireclay and high-alumina refractory brick, ASTM, West Conshohocken, 2022.

[15] ASTM C67/C67M-21, Standard test methods for sampling and testing brick and structural clay tile, ASTM, West Conshohocken, 2021.

[16] ASTM C133-97(2021), Standard test methods for cold crushing strength and modulus of rupture of refractories, ASTM, West Conshohocken, 2021.

[17] TCVN 6530:3-2016, Test methods – Part 3: Dense shaped refractory products – Determination of bulk density, apparent porosity, water absorption and true porosity, Vietnam Standards and Quality Institute (VSQI), Hanoi, 2016.

[18] TCVN 6530-2:2016, Test methods – Part 2: Determination of true density, Vietnam Standards and Quality Institute (VSQI), Hanoi, 2016.

[19] TCVN 6530:5-2016, Test methods – Part 5: Dense shaped refractory products – Determination of permanent change in dimensions on heating, Vietnam Standards and Quality Institute (VSQI), Hanoi, 2016.

[20] ASTM C155-97(2022), Standard classification of insulating firebrick, ASTM, West Conshohocken, 2022.

[21] Sarkar R., Refractory technology: Fundamentals and Applications, New York: CRC Press, 2017.

[22] Hung N.D., Manufacturing technology of refractories (Vietnamese), Hanoi: Bach Khoa, 2013.

[23] Sittiakkaranon S., and Phonphuak N., Microstructural and physical characterization og cordierite-mullite ceramics refractories, International Journal of GEOMATE, 25(108), 2023, pp. 233-240. https://doi.org/10.21660/2023.108.7577

[24] TCVN 4710:2018, Refractory product - Fireclay brick, Vietnam Standards and Quality Institute (VSQI), Hanoi, 2018.

[25] TCVN 7484:2005, Refractory materials - High alumina bricks, Vietnam Standards and Quality Institute (VSQI), Hanoi, 2005.

[26] Yeh C.-T., and Tuan W.-H., Oxidation mechanism of aluminum nitride revisited, Journal of Advanced Ceramics, 6(1), 2017, pp.27-32. https://doi.org/10.1007/s40145-016-0213-1

[27] Amkpa J.A., Badarulzaman N.A., and Aramjat A.B., Influence of sintering temperatures on physico-mechanical properties and microstructure of refractory fireclay bricks, International Journal of Engineering and Technology, 8(6), 2017, pp.2588-2593. https://doi.org/10.21817/ijet/2016/v8i6/160806214

[28] Surendranathan A.O., An introduction to ceramics and refractories, New York: CRC Press, 2015.

[29] Schneider H., Chreuer J., and Hildmann B., Structure and properties of mullite – A review, Journal of the European Ceramic Society, 28(2), 2008, pp.329-344. https://doi.org/10.1016/j.jeurceramsoc.2007.03.017

[30] Cui K., Zhang Y., Fu T., Wang J., and Zhang X., Toughening mechanism of mullite matrix composites: A review, coatings (MDPI), 10(7), 2020, pp. 1-24. https://doi.org/10.3390/coatings10070672

[31] Aksel C., The effect of mullite on the mechanical properties and thermal shock behaviour of alumina–mullite refractory materials, Ceramics International, 29, 2003, pp. 183-188. https://doi.org/10.1016/S0272-8842(02)00103-7

[32] Bharthasaradhi R., and Nehru L., Structural and phase transition of α-Al2O3 powders obtained by co-precipitation method, Phase Transitions, 89(1), 2015, pp.77-83. https://doi.org/10.1080/01411594.2015.1072628